Clim Dyn (2013) 40:663–675
DOI 10.1007/s00382-012-1403-3

Inverse relationship between the equatorial eastern Pacific annual-cycle and ENSO amplitudes in a coupled general circulation model

Soon-Il An · Jung Choi

Received: 29 October 2011 / Accepted: 15 May 2012 / Published online: 29 May 2012

Abstract We propose a dynamical interpretation of the inverse relationship between the tropical eastern Pacific annual-cycle (AC) amplitude and the El Niño-Southern Oscillation (ENSO) amplitude, based on a pre-industrial simulation of Geophysical Fluid Dynamics Laboratory Couple climate model 2.0 with a fixed concentration of greenhouse gases spanning approximately 500 years. The slowly varying background conditions over more than a decade alternately provided favorable conditions for two opposite regimes, namely the 'strong AC—weak ENSO regime' and the 'weak AC—strong ENSO regime'. For the weak AC—strong ENSO regime, the tropical eastern Pacific shows meridional-asymmetric surface warming with an emphasis on the southern part, leading to weakening of both the zonal trade wind and the cross equatorial southerly wind, as well as deepening of both the thermocline and mixed layer. The deeper mixed layer, weaker southerly wind, and reduced zonal gradient of the mean sea surface temperature due to tropical eastern Pacific warming all acts to reduce the AC. Conversely, the ENSO was intensified by the deeper mixed layer and deeper thermocline depth (thermocline feedback), but suppressed by the deeper thermocline depth (Ekman feedback) and the reduced zonal temperature gradient. We also computed the coupling strengths of the ENSO and AC, defined as the linear regression coefficients of the zonal and meridional wind stresses against the eastern Pacific SST, respectively. The coupling strengths of both the AC and ENSO are larger when they are intensified, and vice versa. All processes for the weak AC—strong ENSO regime operate in the opposite manner for the strong AC—weak ENSO regime.

Keywords ENSO · Annual cycle · Decadal modulation · Inverse relationship between ENSO and annual cycle

S.-I. An (✉) · J. Choi
Department of Atmospheric Sciences,
Yonsei University, Seoul 120-749, Korea
e-mail: sian@yonsei.ac.kr

1 Introduction

The equatorial eastern Pacific is the main action-center for the interannual variation, the "El Niño-Southern Oscillation (ENSO)", and records a strong annual cycle (AC), even though solar forcing reaches its peak twice a year. Both the ENSO and AC are driven mainly by air–sea interaction (e.g., Bjerkness 1966, 1969; Xie 1994; Li and Philander 1996), and thus a tight dynamical connection between the two phenomena is obvious, even if their dominant time scales are different (Chang et al. 1994; Wang 1994). For example, the amplitude of the ENSO reaches its maximum during the boreal winter (Rasmusson and Carpenter 1982; Galanti and Tziperman 2000; An and Wang 2001) and the ENSO phase is synchronized with the AC (Stein et al. 2011). This may be due to the nonlinear frequency locking of the ENSO to an annual period (Jin et al. 1994; Tziperman et al. 1994) or seasonal changes in the linear stability of the ENSO (Tziperman et al. 1998). Not only is the ENSO influenced by the AC, but it also modifies the strength of the seasonal sea surface temperatures (SST) and wind variations (Xie 1995; An and Choi 2009). For example, the AC tends to be weaker during El Niño periods and stronger during La Niña periods (Gu and Philander 1995; Xie 1995). The interaction between the AC and ENSO in a seasonal-to-annual time scale may be understood by either seasonally varying instabilities (Tziperman et al. 1998; An and Wang 2001; Galanti et al. 2002;

Burgers et al. 2005; An and Choi 2010) or nonlinear interactions via a frequency-entrainment mechanism (Chang et al. 1994; Timmermann et al. 2007a, b).

Recent studies argued for significant covariation between the ENSO and AC beyond a seasonal time scale, such that the decadal change in ENSO amplitude is negatively correlated to that in AC amplitude (Timmermann et al. 2007b), and thus the active ENSO period coincides with the inactive AC period and vice versa. Regardless of changes in the AC and the annual mean, ENSO amplitude can vary with the decadal time scale via a purely nonlinear process, known as 'El Niño bursting' (Timmermann and Jin 2002; Timmermann et al. 2003) or via stochastic excitation within a linearly stable regime with prescribed stochastic forcing (Chang et al. 1996; Eckert and Latif 1997; Blanke et al. 1997; Moore and Kleeman 1999; Wang et al. 1999). However, a slowly-varying background condition also leads to decadal amplitude modulation for the ENSO (An et al. 2010). This is because ENSO characteristics are highly dependent on the climate state (e.g., Jin 1996; Li and Hogan 1999; Fedorov and Philander 2000; An and Jin 2001; Wang and An 2001; An et al. 2006; Bejarano 2006), which is also true for the AC (Xie 1997; An et al. 2010; Timmermann et al. 2004). Therefore, we expect that long-term variation of the climate state can modify both the ENSO and AC, and its influence on the two phenomena would be presumably in opposition, as seen in various climate system models (e.g., Timmermann et al. 2007b; An et al. 2010). An et al. (2010) attributed the inverse relationship between the ENSO and AC amplitudes to slowly-varying background climate conditions. They showed that the long-term mean surface warming in the western Pacific and deepening of the thermocline suppress ENSO activity by reducing the coupled instability and shortening ocean adjustment timescale, leading to quick turnabout, and amplifying the AC by the intensification of a zonal SST gradient. However, a more comprehensive understanding of this relationship needs to be pursued.

This study is an extension of An et al. (2010), focusing on the relevant mechanism in the inverse relationship between the ENSO and AC amplitudes, using the long-term simulation of GFDL CM2.0 for pre-industrial climate conditions. An et al. (2010) utilized a greenhouse warming experiment obtained from the Max Planck Institute for Meteorology Coupled General Circulation Model (ECHAM5/MPI-OM1), in which the inverse relationship under warm climate conditions actually becomes more significant. Conversely, we focused on natural variability without imposing any external forcing, and thus demonstrate that this inverse relationship is naturally driven. In Sect. 2, we introduce the model utilized. In Sect. 3, we describe our analysis of the relationship between the ENSO and the annual cycle amplitude using correlation methods. The SST equations for AC and ENSO are introduced in Sect. 4. The possible mechanisms are proposed in Sect. 5 and we discuss other processes in Sect. 6. In Sect. 7, we present our final conclusions.

2 GFDL CM2.0

We used one long-term simulation of the GFDL CM2.0 model, spanning over 500 years, to address why the ENSO and annual cycle amplitudes change in opposite directions. This particular simulation was performed under pre-industrial conditions such that the CO_2 concentration was fixed at 280 ppmv. The data are available from the PCMDI or GFDL at http://nomads.gfdl.noaa.gov/CM2.X/.

The ocean component of this model used a $1^\circ \times 1^\circ$ horizontal B-grid telescoping to 1/3 meridional spacing near the equator and 50 vertical layers, based on the Modular Ocean Model version 4 (MOM4) code (Wittenberg et al. 2006). It includes an explicit free surface with true freshwater fluxes exchanged between the atmosphere and ocean. The surface wind stress was calculated using the velocity of the surface wind relative to the surface currents. Its atmospheric component used a B-grid dynamical core with a horizontal resolution of 2° latitude by 2.5° longitude grid spacing for 24 vertical levels. The atmospheric model consisted of a relaxed Arakawa-Schubert parameterization (Moorthi and Suarez 1992) for its convection scheme and a simple local parameterization of the vertical momentum transport by cumulus convection. No flux adjustment was applied. The model formulations are described in detail by Delworth et al. (2006), and Wittenberg et al. (2006) provide generally realistic performances of the tropical Pacific climate using this model.

To check the model's performance for simulating tropical Pacific climate variability, we compared the annual cycle and dominant patterns of the observation and the model. For the observation, we used the Simple Ocean Data Assimilation (SODA) reanalysis set (Carton et al. 2005; Carton and Giese 2008) spanning from January 1871 to December 2008, showing monthly averages. Similar to the atmospheric reanalysis projects, the aim of the SODA reanalysis project was to reconstruct historical ocean climate variability over space and time. Version 2.2.4 of SODA, the most recently released version, is mapped onto a uniform $0.5^\circ \times 0.5^\circ$ grid. The SODA data were built by interpolating unevenly distributed ocean measurements into three-dimensional global fields of temperature, salinity, and current velocity using an ocean general circulation model. Overall the annual cycle over the equatorial eastern Pacific was reasonably well simulated (Fig. 1), showing warming during the boreal spring, cooling during the boreal fall, and the characteristic westward propagation of SST

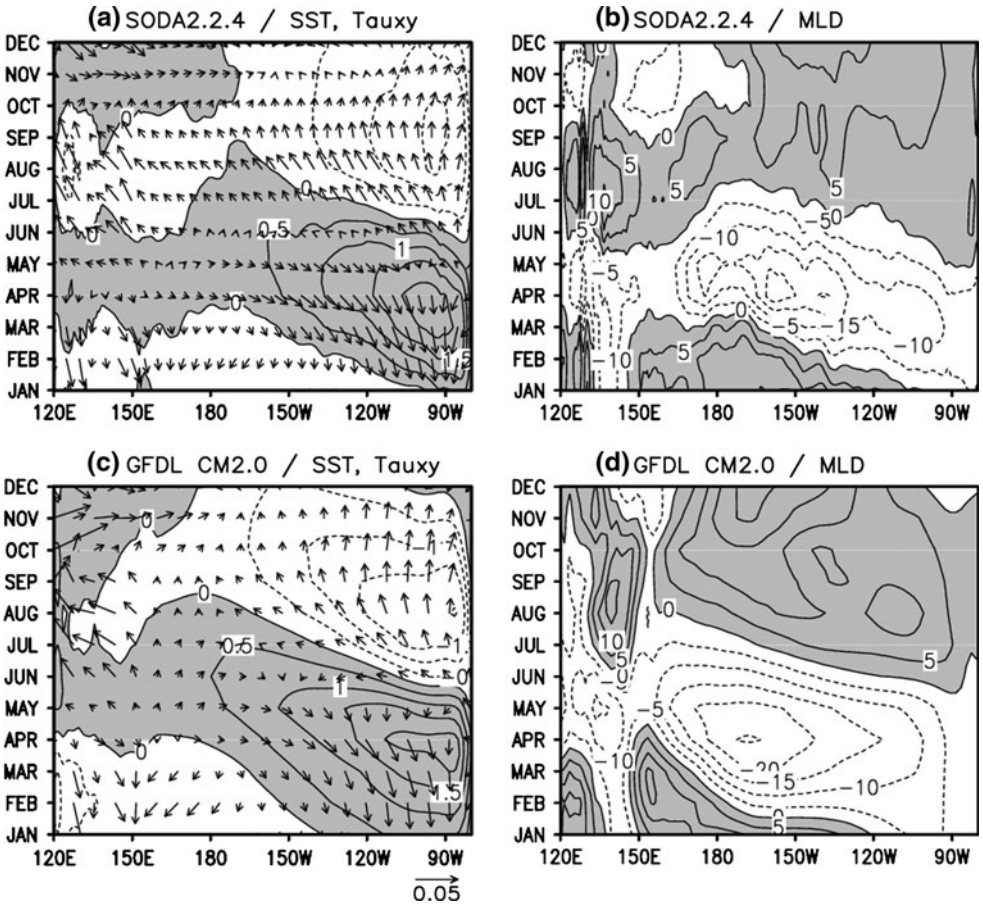

Fig. 1 Time-longitude evolution along the equatorial band (5°S–5°N) of: **a** the climatological SST (°C) and surface zonal and meridional wind stresses (Nm^{-2}) and **b** the mixed layer depth (m) obtained from SODA. **c** and **d** as in (**a**) and (**b**), respectively, except from GFDL CM2.0. Annual mean values have been removed to highlight the annual cycle. Positive values are *shaded*

anomalies. The amplitude of the annual cycle in SST was also reasonable, in that it reached up to approximately two degrees and down to approximately −1.5°. The annual changes in the trade winds were dynamically consistent, showing the weakening and intensifying of wind speeds during the spring and fall, respectively. The meridional component variations of the trade winds accompanied the local SST changes over the eastern Pacific through the upwelling changes. Meanwhile, the zonal component variations of the trade winds were attributed to the westward propagation of SST in the AC time scales (An et al. 2010).

The mixed layer depth (hereafter, MLD) also showed a clear annual cycle. Here, MLD is defined as the depth at which the temperature differs by 0.5 °C from the surface temperature, as in Monterey and Levitus (1997). The annual cycle in the MLD over the eastern equatorial Pacific was generated by the mechanical mixing, accompanied by the surface wind stress or the convection via density changes. Therefore, the annual variations in both the SST and the MLD were driven by wind stress. Thus, the amplified wind stress during the fall led to the surface cooling, as well as the deepening of the MLD through the intensified upwelling and mixing. Conversely, reduced wind stress during the spring led to a surface warming and shoaling of the MLD through a reduced upwelling and mixing. Even the MLD in the model was similar to that of the observation, except that the model mixed layer in the eastern Pacific between 120° and 100°W was deeper during the late summer, which may result in earlier cooling than what was observed.

To identify the dominant SST variation, an empirical orthogonal function analysis (EOF) was applied to the tropical Pacific SST. The total mean for the entire data period was removed before applying the EOF. As seen in Fig. 2a, the first EOF pattern was identified as a meridionally asymmetric mode with maximum loading at the equatorial eastern Pacific, which was an annual cycle mode (Wang 1994; Kim and Chung 2001). The principal component (PC) of the first EOF mode was dominated by a near annual band, in both observations and the model as seen in the time series and power spectral density distribution. Positive and negative peaks appeared in March and September, respectively. The second EOF pattern exhibited a maximum in the equatorial eastern Pacific (Fig. 2b). The second EOF mode was dominated by an interannual variation, i.e., ENSO, but still contaminated by an AC. These results are almost identical to those of Wang (1994). This mode can be interpreted as the combination of the equatorially symmetric AC and ENSO. Because of the seasonal

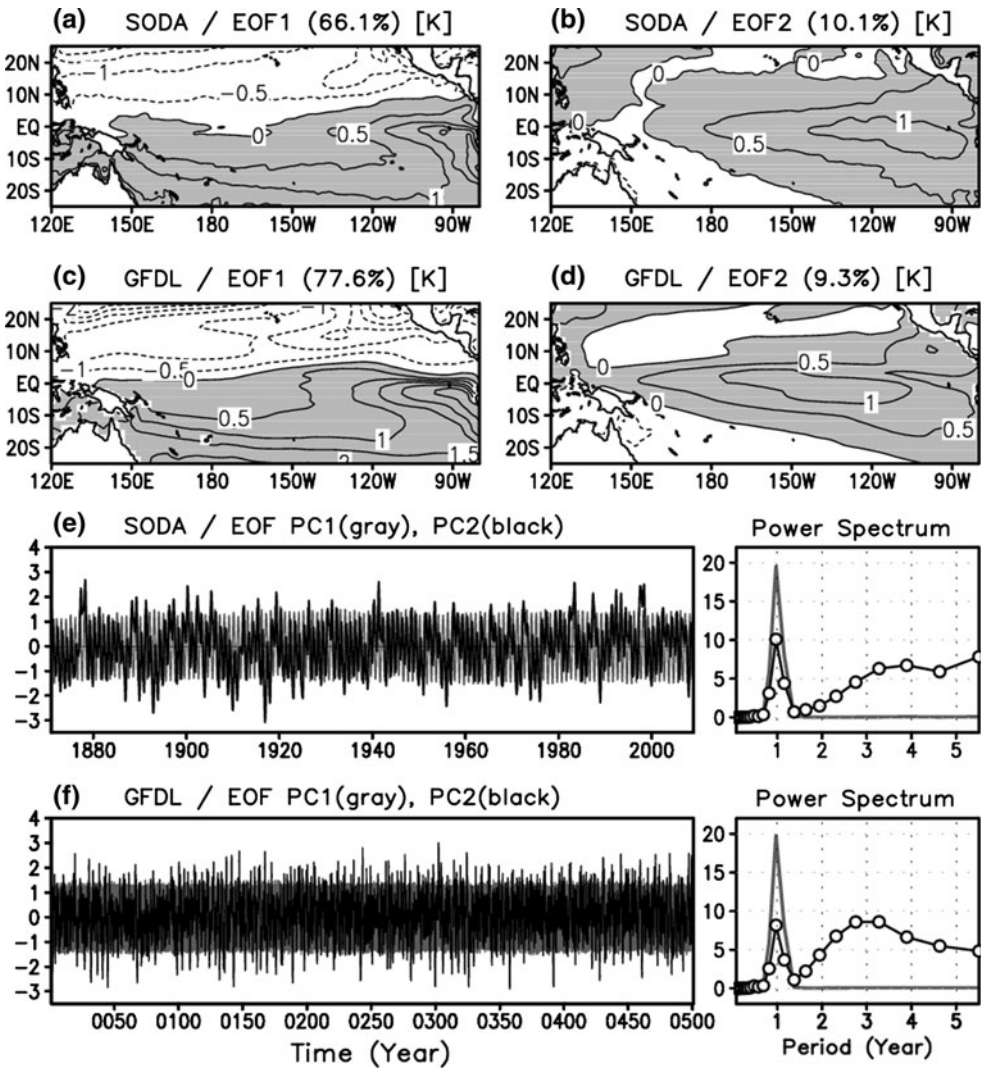

Fig. 2 **a** First and **b** second EOF patterns of the SST obtained from SODA. **c** and **d** as in (**a**) and (**b**), respectively, except from GFDL CM2.0. Each eigen vector has been multiplied by the corresponding eigen value and the standard deviation of PC time series. The percentage variance that explains each mode is shown in the *upper right corner* of each panel. The positive values are *shaded*. **e** The normalized PC time series of the first and second EOF from SODA and the power spectrum density (first mode: *gray solid line*; second mode: *open-circle*). **f** Same as (**e**) but for GFDL CM2.0. Units for (**a**)–(**d**) are [K]

locking nature of the ENSO and their spatial similarities, the symmetric AC and ENSO signals were barely separated (An and Choi 2010). The first and second EOF modes obtained from the observation accounted for 66 and 10 % of the total variance, respectively. As seen in Fig. 2c, d, the first and second EOF patterns in the model, which accounted for 78 and 9 % of the total variance, respectively, were similar to their observed counterparts. Therefore, more than 75 % of the SST variance explained by the leading modes was captured by the model, indicating that the model simulation is valid for use in this study.

3 Long-term changes in the annual cycle and ENSO amplitude

We examined the temporal evolution of the equatorial eastern Pacific SST time series averaged over the Niño-3 region (5°S–5°N, 150°–90°W) (Fig. 3a). This SST variation was mostly dominated by the annual cycle and the ENSO, and its mean and standard deviation were 24.69 and 1.37 °C, respectively. It varied between 20.01 and 28.66 °C, with its amplitude reaching approximately eight degrees. To extract variations of the ENSO and AC amplitudes, Morlet wavelet analysis (Torrence and Compo 1998) was applied to the Niño-3 SST shown in Fig. 3a. The decadal-to-multidecadal variations in the annual bands, as well as in the interannual bands associated with the ENSO, were pronounced (Fig. 3b). Taking the 20-year sliding average of the scale-averaged wavelet power for the annual band (0.8–1.2 years) and interannual band (2–7 years), we were able to identify indices for the AC amplitude and the ENSO amplitude, respectively. In Fig. 3, the two indices represent a clear out-of-phase relationship with the correlation coefficient of −0.46 (where the first and last 10 years are excluded from the correlation), which is statistically significant at a 90 % confidence level. Previous studies confirmed that both the observed and simulated changes in ENSO amplitude were

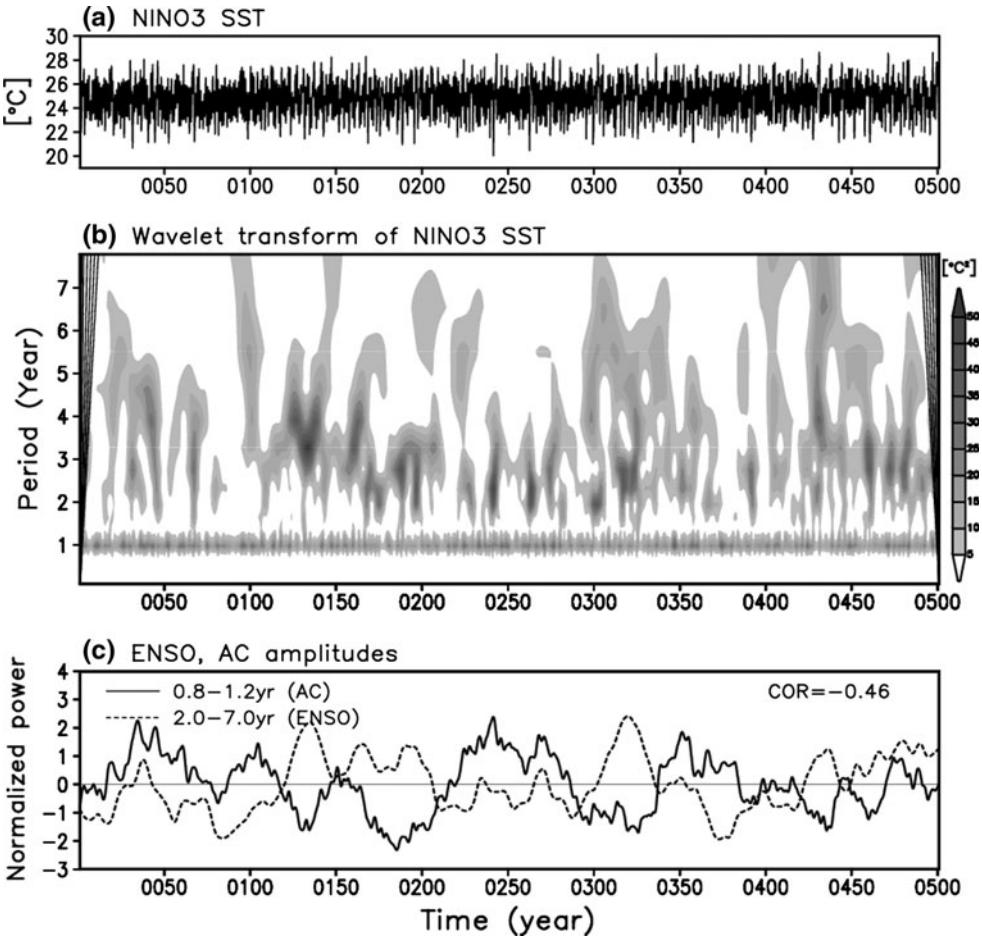

Fig. 3 **a** Time series of Niño-3 (150°–90°W, 5°S–5°N) SST obtained from the GFDL CM2.0 preindustrial run and **b** its corresponding wavelet spectrum. **c** Time series of the 20-year sliding average of the scale-averaged wavelet power over the 2–7 year band (i.e., interannual band or ENSO; *dotted line*), and over the 0.8–1.2 year band (i.e., annual cycle band; *solid line*) for the Niño-3 SST. The Morlet wavelet spectrum is used (Torrence and Compo 1998)

negatively correlated to changes in the annual cycle strength in the eastern equatorial Pacific (Gu and Philander 1995; Xie 1995; Fedorov and Philander 2001; Guilyardi 2006; Timmermann et al. 2007b; An et al. 2010). This negative correlation suggests the existence of two different climate states—a strong AC/weak ENSO and a weak AC/strong ENSO regime.

To depict the background conditions associated with the long-term changes in the AC and ENSO amplitudes, we computed a linear regression map of the physical variables against the AC and ENSO amplitude indices obtained from the previous wavelet analysis. The warm eastern Pacific and cold western Pacific were appeared during the strong ENSO period, and the zonal trade wind was slightly weaker (Fig. 4a, b). The anomalous northerly wind was dominant, and we also observed north–south asymmetry in the SST, namely the positive SST anomaly over the southeastern Pacific ($\sim$10°S) and the negative or weak positive anomaly over the northeastern Pacific ($\sim$10°N). Both the MLD and thermocline (i.e., 17 degree isotherm) depth became slightly deeper over the eastern Pacific and shallower over the central Pacific (Fig. 4c). The relatively small signal in the thermocline is related to the small change in the trade wind. Figure 4d shows the changes in the equatorially-averaged (5°S–5°N) subsurface temperatures associated with the ENSO amplitude index, and the upper (lower) solid, thick contours represent the climatology of the MLD (thermocline depth). In the subsurface, warming slightly above the mean thermocline over the eastern Pacific and cooling over the western Pacific were concurrent with the active ENSO period.

Conversely, the regression maps of the AC amplitude index show opposite phenomena to those of the ENSO amplitude index. They show the cold surface, the intensified zonal trade and southerly winds, slightly shallower MLD and thermocline depths, and subsurface cooling over the eastern Pacific (Fig. 4e–h). The regression patterns against the AC amplitude index were mirror images of those against ENSO amplitude index. For instance, the spatial correlation between the SST (subsurface temperature) regression map associated with ENSO amplitude index and that with AC amplitude index was −0.76 (−0.77). Therefore, the mean background conditions led to an inverse relationship between the AC and ENSO amplitudes, as proposed by An et al. (2010). In the next sections, we propose potential physical mechanisms for the

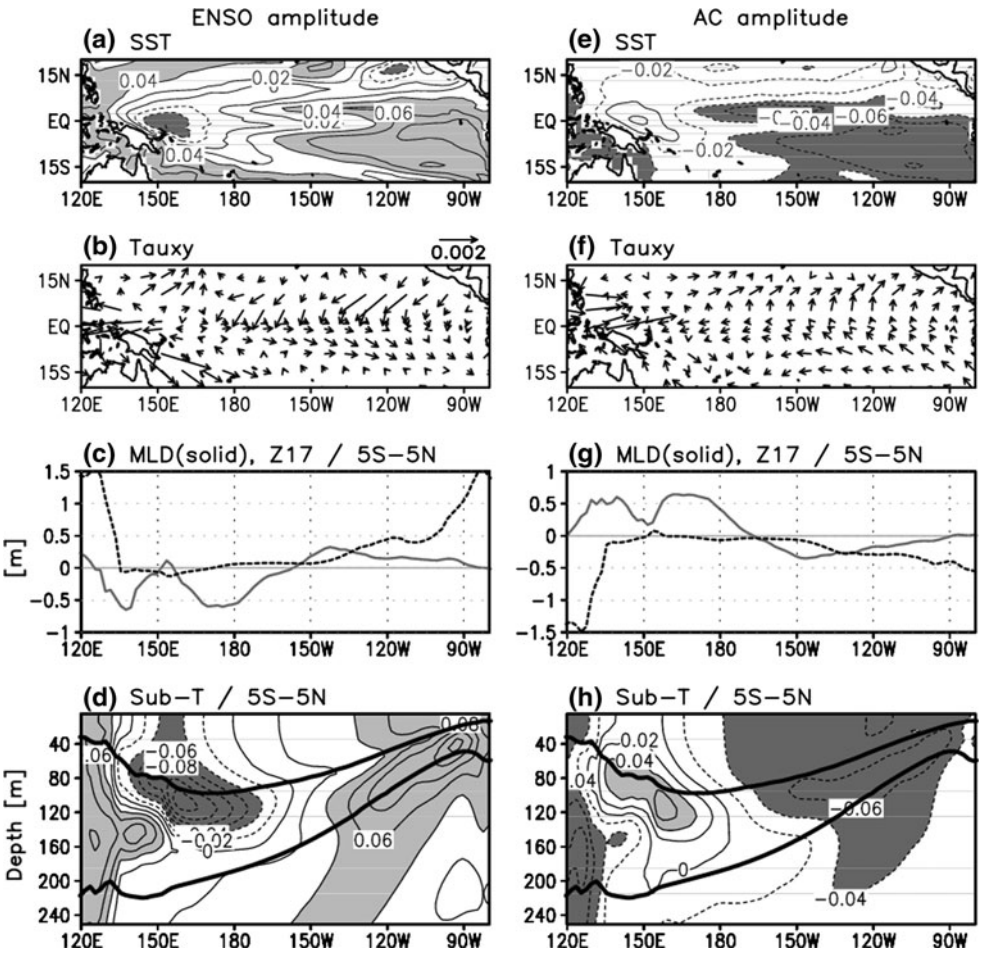

Fig. 4 Linear regression maps of **a** SST, **b** wind stress, **c** the mixed layer depth and 17 °C isotherm depth, and **d** the equatorial ocean temperature anomalies averaged over the equatorial band (5°S–5°N) with respect to the ENSO amplitude index. The ENSO amplitude index indicates the time series in Fig. 3c (*dotted line*). The *solid* and *dashed lines* in (**c**) indicate the mixed layer depth and 17 °C isotherm depth, respectively. **e**–**h** as in (**a**)–(**d**), respectively, except for the regression maps against to annual cycle amplitude index, which is the time series in Fig. 3c (*solid line*). In (**d**) and (**h**), the *upper* (*lower*) *thick solid line* represents the climatology of the mixed layer depth (17 °C isotherm depth). Greater than 0.04 and smaller than −0.04 are *light-* and *dark-shaded*, respectively

background conditions responsible for the inverse relationship between the AC and ENSO amplitudes.

4 Equations for AC and ENSO amplitude

Before discussing the physical mechanism, here we introduce the amplitude tendency equations for AC and ENSO. These equations will be utilized in the next section to address the possible mechanism.

4.1 AC amplitude equation

The SST equation for the annual cycle over the equatorial eastern Pacific was developed by Xie (1994) as follows:

$$\frac{\partial T'}{\partial t} = -(\bar{u}_O - c)\frac{\partial T'}{\partial x} + \frac{2Q_S}{\rho C_p h} - \left(1 + \frac{\eta}{H}\right)\frac{2\bar{Q}_E}{\rho C_p h}\frac{\bar{v}}{|\bar{u}|^2}v' - \varepsilon T', \tag{1}$$

where h is the mixed layer depth, c is the phase speed determined by the air–sea interaction, $\bar{u}_o$ is the mean zonal current; η/H is a parameter for the relative importance between the latent heat flux and vertical mixing; Q_s and $\bar{Q}_E$ are the perturbation solar radiation and the mean latent heat flux, respectively, and $\bar{u}$ and $\bar{v}$ are the mean zonal and meridional winds, respectively. The first term on the right-hand side indicates westward propagation via the surface air–sea coupling; the second and third terms indicate the surface solar radiation and the latent heat flux depending on changes in the meridional wind, respectively. All parameters are taken as positive values, and other details for Eq. (1) can be found at Xie (1994).

To derive the amplitude tendency equation, T' is multiplied at Eq. (1). Then, we have:

$$\frac{\partial}{\partial t}\langle T'^2\rangle = -(\bar{u}_O - c)\frac{\partial}{\partial x}\langle T'^2\rangle + \frac{4}{\rho C_p h}\langle Q_s T'\rangle - \left(1 + \frac{\eta}{H}\right)\frac{4\bar{Q}_E}{\rho C_p h}\frac{\bar{v}}{|\bar{u}|^2}\langle v'T'\rangle - 2\varepsilon\langle T'^2\rangle, \tag{2}$$

where $\langle\cdot\rangle$ indicates the temporal average for a certain period. As seen in Eq. (2), the amplitude of the AC increases when the solar forcing and SST are positively correlated, and the meridional wind and SST are negatively correlated.

4.2 ENSO amplitude equation

The SST equation for ENSO over the equatorial Pacific is developed from an intermediate atmosphere–ocean coupled model for ENSO (e.g., Zebiak and Cane 1987; Battisti 1988) as followings:

$$\frac{\partial T'}{\partial t} = -u'\frac{\partial(\bar{T}+T')}{\partial x} - \bar{u}\frac{\partial T'}{\partial x} - v'\frac{\partial(\bar{T}+T')}{\partial y} - \bar{v}\frac{\partial T'}{\partial y} - \delta\{\Delta(\bar{w}+w') - \Delta(\bar{w})\}\frac{\partial \bar{T}}{\partial z} - \delta\{\Delta(\bar{w}+w')\}\frac{\partial T'}{\partial z} - \alpha T' \quad (3)$$

where T is the SST; u, v are zonal and meridional currents; w is the surface layer upwelling velocity; δ is the efficiency coefficient for the upwelling (here $\delta = 1$); $\Delta(x) = x$, when $x > 0$, otherwise $\Delta(x) = 0$; α is a thermal damping coefficient including all thermodynamical processes at the ocean surface. The upper bar and prime indicate the mean and perturbation quantities in the ENSO time scale, respectively. The first two terms of the right hand side indicate the zonal thermal advection; the second two terms indicate the meridional thermal advection; and the third two terms indicate the vertical thermal advection.

When $\bar{w} \gg w'$ and $\bar{w} > 0$, which is usual for the ENSO and climatological mean over the tropical eastern Pacific, then the upwelling term of Eq. (3) can be approximated as

$$\frac{\partial T'}{\partial t} \approx -u'\frac{\partial(\bar{T}+T')}{\partial x} - \bar{u}\frac{\partial T'}{\partial x} - v'\frac{\partial(\bar{T}+T')}{\partial y} - \bar{v}\frac{\partial T'}{\partial y} - w'\frac{\partial \bar{T}}{\partial z} - \bar{w}\frac{\partial T'}{\partial z} - \alpha T' \quad (4)$$

As in AC equation, in order to derive the amplitude tendency equation, T' is multiplied at Eq. (4). Then, we have:

$$\frac{\partial}{\partial t}\langle T'^2\rangle \approx -\bar{u}\frac{\partial\langle T'^2\rangle}{\partial x} - 2\langle u'T'\rangle\frac{\partial \bar{T}}{\partial x} - 2\left\langle u'T'\frac{\partial T'}{\partial x}\right\rangle - \bar{v}\frac{\partial\langle T'^2\rangle}{\partial y} - 2\langle v'T'\rangle\frac{\partial \bar{T}}{\partial y} - 2\left\langle v'T'\frac{\partial T'}{\partial y}\right\rangle - \bar{w}\frac{\partial\langle T'^2\rangle}{\partial y} - 2\langle w'T'\rangle\frac{\partial \bar{T}}{\partial z} - 2\alpha\langle T'^2\rangle. \quad (5)$$

5 Possible mechanisms

In this section, we address how the inverse relationship of the AC-ENSO amplitude can be attributed to the background conditions, specifically, the roles of the MLD (together with thermocline depth), zonal trade wind, meridional trade wind and SST. The mean difference of each variable between 'strong' and 'weak' periods has been computed from the composite of each period. The 'strong' and 'weak' periods are defined when the normalized time series of Fig. 3c are greater and less than 1.0 standard deviation, respectively.

5.1 MLD and thermocline depth

We confirmed that the deeper MLD was associated with the small AC (large ENSO) amplitude period (Fig. 4). The deeper MLD suppresses AC amplitude, because the growth rate of the AC is linearly proportional to the net surface heat flux $\left(Q_{net} \approx Q_S - \overline{Q_E}\right)$, but inversely proportional to the MDL (h) [i.e., $\frac{dT}{dt} \propto \frac{Q_{net}}{h}$, also see Eq. (1)]. In the AC time scale, the latent heat flux and vertical mixing play an important role in changing the SST. Both the latent heat flux and vertical mixing are proportional to the surface wind speed (Xie 1994). A deeper mean MLD denotes greater ocean thermal inertia. As a result, the sensitivity of the oceanic response to the surface wind may not be as high as in a normal condition, which results in a small amplitude of the AC of SST. The mean MLD for the strong AC period is shallower than that for the weak AC period by about 46 cm over the Nino-3 region, which is on the order of 1 % of the annual mean depth, yet 10 % of the annual cycle range of MLD. Conversely, the net surface heat flux in the ENSO time scale ('anomalous heat flux') acts as linear damping, where the damping rate is proportional to the SST anomaly and inversely proportional to the MLD (e.g., Zebiak and Cane 1987). In other words, when the MLD is deeper than normal, El Niño decays slowly, as the deeper MLD has longer oceanic memory. Therefore, the deeper MLD can intensify the ENSO amplitude and vice versa.

As indicated in Fig. 4, the thermocline depth changed in the same direction as the MLD. We focused here on the ENSO rather than the AC, because the AC is decoupled from the thermocline depth (Xie 1994). The thermocline depth is related to the subsurface ocean temperature. Since subsurface ocean water is actually transported into the mixed layer when upwelling occurs, the vertical thermal advection in the SST tendency equation alters with changes in the thermocline depth. The vertical thermal advection terms in the anomalous SST tendency equation over the eastern Pacific are the fifth and sixth term of the right hand side of Eq. (4), which can be further approximated, based on a dominant physical process. Firstly, the anomalous vertical velocity can be approximated as; $w' \propto -\tau'_X \propto -T'$ (Choi et al. 2009), where τ'_X is the surface zonal wind stress, and thus, the first term of the vertical thermal advection becomes $-w'\frac{d\bar{T}}{dz} \propto T'\frac{d\bar{T}}{dz}$. The second term can also be approximated as; $-\bar{w}\frac{\partial T'}{\partial z} \approx -\bar{w}\frac{(T'-T'_{sub})}{\Delta z} \approx -\bar{w}\frac{(T'-\gamma D')}{\Delta z}$, where T'_{sub} is the subsurface temperature, and D' is the thermocline depth. In this approximation, an empirical relationship between T'_{sub}

and D' can be applied such as $T'_{sub} \approx \gamma D'$, which is a simple version of the T'_{sub} parameterization used in the intermediate coupled model (Zebiak and Cane 1987; Dewitte 2000; Choi et al. 2009). The γ indicates the effect of thermocline depth change on ocean subsurface temperature. This approach is reasonable, at least for the ENSO time scale (Jin et al. 2006; Kim and Jin 2011). Thus, we were left with $\frac{\partial T'}{\partial t} \propto \frac{\partial \bar{T}}{\partial z} T'$ and $\propto -\frac{\bar{w}}{\Delta z} T' + \frac{\bar{w}\gamma}{\Delta z} D'$, and further manipulation going for the amplitude tendency equation gives birth to $\frac{\partial}{\partial t}\langle T'^2 \rangle \propto \frac{\partial \bar{T}}{\partial z}\langle T'^2 \rangle$ and $\propto -\frac{\bar{w}}{\Delta z}\langle T'^2 \rangle + \frac{\bar{w}\tilde{\gamma}}{\Delta z}\langle D'T' \rangle$ (hereafter A, B, C terms, in a row), where $\langle\rangle$ could be either domain or temporal average and $\langle T'_{sub} \rangle \approx \tilde{\gamma}\langle D' \rangle$.

The A term, i.e., $\frac{\partial \bar{T}}{\partial z}\langle T'^2 \rangle$ (always > 0) is a growing term and its growth rate depends on the mean vertical temperature gradient, $\frac{\partial \bar{T}}{\partial z}$ (always >0), which corresponds to Ekman (upwelling) feedback (Jin et al. 2006). A deeper thermocline depth results in a smaller $\frac{\partial \bar{T}}{\partial z}$ (i.e., small stratification) and thus the growth rate by this effect is reduced. The mean vertical temperature gradient $\frac{\partial \bar{T}}{\partial z}$ for the strong ENSO period (i.e., corresponding to deeper thermocline) is smaller than that for the weak ENSO period by about 0.02 °K $(100\ \text{m})^{-1}$ (about 0.3 % of total mean value) over Nino-3 region, where is obtained from difference between the vertical averaged ocean temperature over 0–50 m depth (i.e., mixed layer temperature) and the ocean temperature at 55 m depth.

The change in the mean thermocline depth also influences the C term, which corresponds to thermocline feedback (An and Jin 2001; Jin et al. 2006), especially by modifying γ, which is again a conversion parameter between the thermocline depth anomaly and the subsurface temperature anomaly. In general, γ is inversely proportional to the mean thermocline depth (Zebiak and Cane 1987; Dewitte 2000). This is due to the fact that, as the mean thermocline deepens, the subsurface temperature (i.e., ocean temperature right-below the mixed layer depth) becomes less sensitive to changes in the anomalous thermocline. Therefore, A and C terms modified by the mean thermocline are supposed to lead to a reduction of the ENSO amplitude as the mean thermocline deepens. This has been verified by the linear stability analysis by Choi et al. (2009) (see Fig. 9 of Choi et al. 2009), which showed that the growth rate, computed using the linearized intermediate coupled model, was reduced when the deeper mean thermocline depth was applied. However, γ is not solely determined by the mean thermocline depth but by the nonlocal process of ocean dynamic adjustment as well as air–sea coupling process. The $\tilde{\gamma}$ for the strong ENSO period is greater than that for the weak ENSO by about 0.022 °K m^{-1} (about 22 % of total mean value). Here the $\tilde{\gamma}$ of $\langle T'_{sub} \rangle \approx \tilde{\gamma}\langle D' \rangle$ where $\langle\cdot\rangle$ indicates the spatial average over Nino-3 region, is estimated for the strong and weak ENSO periods, separately. On the whole, the deeper thermocline suppresses the Ekman feedback (A term), while intensifies the thermocline feedback (C term). Quantitatively the increased thermocline feedback seems to be larger than the decreased Ekman feedback, but the net effect of the thermocline is hardly determined.

The B term is a damping term and its damping rate depends on the mean upwelling velocity, $\bar{w}$ (always >0), and thus the strong (weak) upwelling leads to strong (weak) damping of ENSO. The mean upwelling at 50 m depth for the strong ENSO period is weaker than that for the weak ENSO period by about 2.0×10^{-6} cms^{-1} over Nino-3 region. However, such change can be offset by change in C term, i.e., thermocline feedback, because both terms commonly include the mean upwelling but act in opposite way. This because the thermocline and SST anomalies over the eastern Pacific are positively correlated, i.e., $\langle D'T' \rangle > 0$, especially during the mature phase of ENSO (Zelle et al. 2004), and thus the C term is mostly positive during the ENSO evolution, indicating it acts as positive feedback, and proportional to the intensity of mean upwelling.

5.2 SST and surface winds

The AC of the SST was initiated near the eastern coastal region, and then propagated to the west by virtue of the surface air–sea interaction, which is related to the zonal advection of the mean temperature gradient by an anomalous zonal current in the mixed layer (i.e., $-u' d\bar{T}/dx$ where 'prime' and 'upper bar' indicate AC and background mean quantities, respectively) (Xie 1994) (Fig. 1). Therefore, the reduction (intensification) of the zonal gradient of the mean SST ($d\bar{T}/dx$) resulted in suppression (enhancement) of the AC, especially for the propagation part of the AC over the central Pacific (An et al. 2010). In the SST equation for the AC, the first term in the right hand side of Eq. (1) indicates the westward propagation of the AC. As shown in Fig. 4, the warmer mean tropical eastern Pacific, i.e., decreasing of the zonal gradient of the mean SST, corresponds to a weak AC period and vice versa. Regarding the ENSO time scale, the smaller $d\bar{T}/dx$ reduces the 'zonal advection feedback' (An et al. 1999; Jin and An 1999). The zonal advection feedback destabilizes the SST mode, which is driven by the surface air–sea interaction without invoking subsurface process (An and Jin 2001; Jin et al. 2003). Therefore, like the AC, the westward propagation of the SST anomaly of the ENSO is supposed to be suppressed when $d\bar{T}/dx$ is reduced. However, the equatorial Pacific surface warming leads to more active

convection over the same region than does cooling and as a result, a local strong air–sea coupling increases over the eastern Pacific (Choi et al. 2009, 2011). Due to this intensified air–sea coupling strength, the warmer surface climate state intensifies the amplitude of the ENSO.

The background state of the enhanced surface meridional wind corresponds to the stronger AC period and vice versa (Fig. 4). As in Eq. (2), a change in the mean meridional wind ($\bar{v}$) influences the amplitude of the AC by modifying the surface latent heat flux. As the meridional wind and SST are negatively correlated in the annual time scale ($\langle v'T' \rangle < 0$), an increase in the mean meridional wind results in large AC amplitude. In other words, when the mean wind speed is larger, the latent heat flux becomes more sensitive to changes in wind speed. The mean meridional surface wind stress (southerly) for the strong AC period is stronger than that for the weak AC period by about 0.08×10^{-2} Nm^{-2} (about 6 % of the annual mean value). Thus, the AC can be amplified under the intensified southerly wind. The opposite is also true.

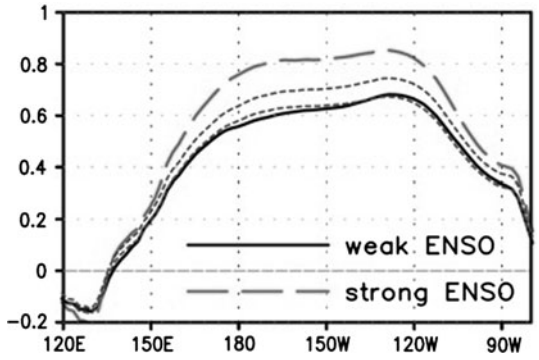

Fig. 5 Air–sea coupling strength for the strong (*long-dashed line*) and weak (*solid line*) ENSO periods. Coupling strength is defined as the regression of SST anomaly over the equatorial band (domain average between 5°S and 5°N) against the zonal wind stress anomaly index (domain averaged zonal wind stress over 120°E–120°W, 5°S–5°N minus that over 120°–80°W, 5°S–5°N). Units are [K]. *Two dotted lines* indicate 2.5 and 97.5 % ranking of the probability density function obtained from bootstrap method, and thus outer area of the *dotted lines* belongs to above the 95 % confidence level

5.3 Air–sea couplings for the AC and ENSO

In the previous two subsections, we described dynamic interpretations of how background conditions influence AC and ENSO amplitudes. These interpretations, however, might be limited by a lack of air–sea coupling process involved in the AC and ENSO. Measuring the air–sea coupling strength accounts for all of the possible effects that the background conditions may influence in terms of changes in the AC and ENSO amplitudes. In order to examine the effects of the background conditions, we defined two different climate states—strong AC/weak ENSO and weak AC/strong ENSO amplitude periods—based on the AC amplitude index as mentioned previously.

Here, the air–sea coupling strength for the ENSO is defined as the regression of SST anomaly against the wind stress index, where the wind stress index is the difference in the domain averaged zonal wind stress between 120°E–120°W, 5°S–5°N and 120°W–80°W, 5°S–5°N. These two locations have shown a distinct dipole pattern in correlation maps of zonal wind stress anomalies against the Niño-3 index (i.e., SST anomaly averaged over 150°–90°W, 5°S–5°N). The air–sea coupling strength was computed for the weak AC/strong ENSO and strong AC/weak ENSO periods separately. In Fig. 5, the dashed and solid lines indicate the regression coefficient during the strong and weak ENSO periods, respectively. The higher regression coefficient between 180° and 120°W was more pronounced for the strong ENSO period than for the weak ENSO period, inferring that stronger air–sea coupling strength in the equatorial Pacific leads to a strong ENSO.

The air–sea coupling strength for the AC was also defined as the regression of SST anomaly in the AC time scale against the wind stress index. For the AC, the meridional wind stress was used, because changes in the meridional wind stress influence AC amplitude more than change in the zonal wind stress, as it modifies the latent surface heat flux [the third term of the right hand side of Eq. (2)]. Therefore, the linear regression coefficients of the SST against the meridional wind stress index encompassed all of the effects due to changes in the mean mixed layer depth, mean winds, and mean latent heat flux. Here, the wind stress index is defined as the domain averaged meridional wind stress over 160°–80°W, EQ-10°N. The domain was determined based on the correlation map of the meridional wind stress against the equatorial eastern Pacific SST, averaged over 120°–80°W, 5°S–5°N, where the action center of the AC is located. We computed the regression coefficient of the domain averaged SST over 150°–80°W, 5°S–5°N against the meridional wind index for each calendar month for strong and weak AC periods separately; thus, the seasonality of the coupling strength could be determined. As shown in Fig. 6, there was a strong negative relationship between the SST and meridional wind stress (i.e., $\langle v'T' \rangle < 0$), especially in the boreal spring and fall. There also exists a difference in the air–sea coupling strength between the strong and weak AC periods, which becomes distinct from August through October. This difference is marginal during the rest of the year. Thus, during the boreal fall, for the strong AC period, the magnitude of SST cooling is larger than that for the weak AC period, if the anomalous meridional wind stress is not changing. This leads to an intensification of AC amplitude.

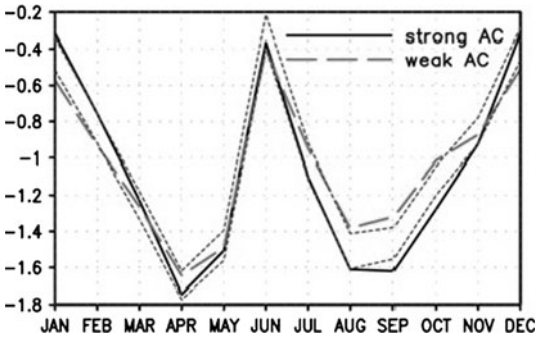

Fig. 6 Air–sea coupling strength for each calendar month for the strong (*solid line*) and weak (*long-dashed line*) AC periods. Coupling strength is defined as the regression of SST over the equatorial eastern Pacific (domain average over 150°–80°W, 5°S–5°N) against the meridional wind stress index (domain averaged meridional wind stress over 160°–90°W, 0°–10°N). Units are [K]. *Two dotted lines* indicate 2.5 and 97.5 % ranking of the probability density function obtained from bootstrap method, and thus outer area of the dotted lines belongs to above the 95 % confidence level

As expected, the coupling strength is larger for the strong AC period.

6 Discussion

The background conditions for the weak AC/strong ENSO period were dynamically consistent with each other, as were those for the strong AC/weak ENSO period. For example, for the weak AC/strong ENSO period, the eastern Pacific warming reduced the zonal gradient of the SST, which led to a weakening of the zonal wind, especially over the central Pacific (e.g., Lindzen and Nigam 1987). The zonal contrast of the thermocline was maintained by the surface stress of the zonal wind; thus, the weakening of the zonal wind caused deepening of the thermocline over the eastern Pacific. Concurrently, the reduced upwelling over the eastern Pacific by virtue of the weak zonal wind led to further surface warming, known as 'Bjerkness feedback' (Bjerkness 1966, 1969). The thermocline could have been uniformly deepened down over the eastern Pacific due to the reduction of the zonal trade wind; however, the SST did not increase uniformly, rather a relatively strong response appeared over the southeastern Pacific. This is because the mean thermocline south of the equator is shallower than that north of the equator, so the SST south of the equator is more sensitive to changes in the thermocline. Therefore, the deepening of the thermocline resulted in more warming south of the equator than north, which finally generated the northerly wind. The northerly wind blew against the mean meridional trade wind, reducing wind speed. In this regard, we expected a shoaling of the MLD because of reduced mechanical turbulence; however, such shoaling was not observed. Conversely, reduced stratification due to subsurface warming (see Fig. 4d, h) increases the efficiency of the mechanical turbulence in driving MLD. Thus, the deepening of the MLD due to stratification changes may overcompensate for the shoaling of the MLD due to the reduced wind speed. The background conditions for the strong AC/weak ENSO were also consistent with each other, for the aforementioned reasons but as in opposite way. In the previous section, we focused on how background conditions influence AC and ENSO amplitudes. However, the background conditions can be modified by both the AC and ENSO (An and Choi 2009, 2010; An et al. 2010; Choi et al. 2009). For example, the residuals produced by the asymmetric oscillatory nature of ENSO were rectified in the background state (An 2009). This rectification effect can be verified by calculating the relationships between skewness and background conditions. We computed 20 years of moving skewness for the Niño-3 index (Fig. 7). The slow-varying skewness and mean SST were positively correlated (0.74). In other words, the ENSO active period corresponded to the background conditions of a warmer eastern Pacific and vice versa; thus, changes in ENSO activity may lead to changes in the background conditions. However, the two-way interactions between the background conditions and the ENSO, including the nonlinear frequency entrainment mechanism between the ENSO and AC (Chang et al. 1994; Xie 1995; Timmermann et al. 2007a, b; Choi et al. 2009) were not investigated in this study.

Our studies took rather qualitative approach, and thus the relative importance between the processes was not quantitatively provided. To make quantitative statement, we need to develop either a diagnostic tool to quantify the contribution of each background climate variable or perform the sensitivity experiment using a coupled model. In case of El Nino, Jin et al. (2006) developed a diagnostic tool to quantify the growth rate of ENSO, so-called 'BJ index', which of the formulation basically resembles the prototype recharge oscillation model. An et al. (2004, 2010) used the linearized version of an intermediate coupled model for ENSO to compute the growth rate and frequency of ENSO for given background climate states. These methods fairly well provide quantitative measure of relative contribution of each process to ENSO, even though these are somewhat constrained by the ways of the formulation and the areal-averaged region. On the while, the method for AC, which is analogous to ENSO's case, has not been introduced yet. Thereby, our approach and result [e.g., Fig. 6; Eq. (2)] will be an appropriate starting point for developing a

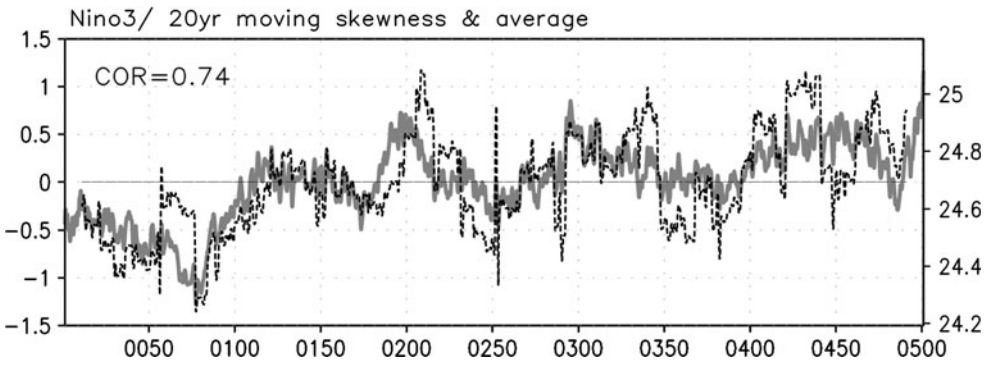

Fig. 7 Time series of a 20-year moving skewness of Niño-3 SST anomaly (*dotted line*) and a 20-year moving average of the SST (*solid line*). Units for skewness and SST are nondimension and °C, respectively

diagnostic tool to quantify the contribution in AC. This will be a future studying subject.

7 Conclusions

Inverse relationships in decadal-to-interdecadal time scales between AC and ENSO amplitudes over the tropical eastern Pacific SST have been observed (Wang 1994) and indicated by CGCMs (Guilyardi 2006; Timmermann et al. 2007b). As in An et al. (2010), the results we obtained using the GFDL CM2.0 showed a negative correlation (−0.46), in the pre-industrial experiment, without any changes in the external forcing. These results were analyzed to address the mechanism underlying the inverse relationship between AC and ENSO amplitudes. In particular, we found that the background conditions of the tropical Pacific, including the MLD, thermocline depth, surface wind and SST, influence changes in the AC and ENSO amplitudes. The proposed mechanisms are summarized as follows.

(a) MLD: MLD is deeper for the weak AC/strong ENSO period and shallower for the strong AC/weak ENSO period. When it is deeper, the AC is suppressed because of increasing heat capacity $\left(\frac{\partial}{\partial t}\langle T'^2\rangle \propto \frac{4}{\rho C_p h}\langle Q_s T'\rangle\right)$, and the ENSO is intensified because of the reduced damping rate.

(b) Thermocline and Upwelling: The thermocline is deeper for the weak AC/strong ENSO period and shallower for the strong AC/weak ENSO period. It may not directly influence the AC, as it does the ENSO. The mean upwelling is weaker for the weak AC/strong ENSO period and stronger for the strong AC/weak ENSO period. When the thermocline is deeper, the ENSO is suppressed because of the reduced positive Ekman (upwelling) feedback due to the reduced mean vertical temperature gradient $\left(\frac{\partial}{\partial t}\langle T'^2\rangle \propto \frac{\partial \bar{T}}{\partial z}\langle T'^2\rangle\right)$, while at the same time the ENSO is enhanced because of the intensified thermocline feedback by the increased subsurface temperature sensitivity to changes in the anomalous thermocline depth $\left(\frac{\partial}{\partial t}\langle T'^2\rangle \propto \frac{\bar{w}\bar{\gamma}}{\Delta z}\langle D'T'\rangle\right)$. The stronger upwelling suppresses the ENSO through the enhanced upwelling cooling $\left(\frac{\partial}{\partial t}\langle T'^2\rangle \propto -\frac{\bar{w}}{\Delta z}\langle T'^2\rangle\right)$, while it intensifies ENSO through the enhanced thermocline feedback $\left(\frac{\partial}{\partial t}\langle T'^2\rangle \propto \frac{\bar{w}\bar{\gamma}}{\Delta z}\langle D'T'\rangle\right)$, and vice versa. Thereby, the net effect is assumed to be small.

(c) SST (zonal SST gradient): The SST is warmer for the weak AC/strong ENSO period and colder for the strong AC/weak ENSO period. When it is warmer, the AC is suppressed because of the reduced zonal thermal advection. For the same reason, the ENSO is also suppressed, particularly that associated with the zonal advection feedback. However, a warmer mean surface condition also leads to a strong air–sea coupling, causing the ENSO amplitude to intensify.

(d) Southerly trade wind: The southerly trade wind is weak for the weak AC/strong ENSO period and strong for the strong AC/weak ENSO period. It may not directly influence the ENSO as it does the AC. When it is weaker, the AC is suppressed because the reduced sensitivity of the latent heat flux to wind changes $\left(\frac{\partial}{\partial t}\langle T'^2\rangle \propto -\left(1+\frac{\eta}{H}\right)\frac{4\bar{Q}_E}{\rho C_p h}\frac{\bar{v}}{|\vec{u}|^2}\langle v'T'\rangle\right)$.

(e) Coupling strength: Coupling strength is defined as the empirical relationship between the SST and zonal trade wind for the ENSO and between the SST and meridional trade wind for the AC. Obviously, for the AC, it is stronger for the strong AC and for the ENSO it is stronger for the strong ENSO and vice versa.

Finally, we proposed that dynamic consistency among the background conditions, including the zonal wind, meridional, SST, thermocline and MLD; the Bjerkness feedback between the zonal trade wind and the tropical eastern Pacific SST maintains a relationship between the suppressed (intensified) zonal trade wind and surface warming (cooling), which requires a deepening (shoaling) of both the thermocline and MLD, and the additional warming (cooling) over the southeastern Pacific due to the deepening (shoaling) of thermocline in the tropical eastern Pacific leads to the suppression (intensification) of the southerly trade wind.

Acknowledgments We acknowledge the modeling groups for providing their data for analysis, the Program for Climate Model Diagnosis and Intercomparison (PCMDI) for collecting and archiving the model output, and the JSC/CLIVAR Working Group on Coupled Modelling (WGCM) for organizing the model data analysis activity. Authors thank F.-F. Jin and A. Timmermann for their valuable comment. This work was supported by the National Research Foundation of Korea (NRF) grant funded by the Korea government (MEST) (No. 2011-0015208).

References

An S-I (2009) A review on interdecadal changes in the nonlinearity of the El Niño-Southern Oscillation. Theor Appl Climatol 97:29–40

An S-I, Choi J (2009) Seasonal locking of the ENSO asymmetry and its influence on the seasonal cycle of the tropical eastern Pacific sea surface temperature. Atmos Res 94:3–9

An S-I, Choi J (2010) Interaction between equatorially symmetric and asymmetric tropical eastern Pacific SSTs. Theor Appl Climatol 102:151–158

An S-I, Jin F–F (2001) Collective role of thermocline and zonal advective feedbacks in the ENSO mode. J Clim 14:3421–3432

An S-I, Wang B (2001) Mechanisms of locking the El Niño and La Niña mature phases to boreal winter. J Clim 27:2164–2176

An S-I, Jin F–F, Kang I-S (1999) The role of zonal advection feedback in phase transition and growth of ENSO in the Cane-Zebiak model. J Meteorol Soc Jpn 77:1151–1160

An S-I, Timmermann A, Bejarano L, Jin F–F, Justino F, Liu Z, Tudhope AW (2004) Modeling evidence for enhanced El Nino-Southern Oscillation amplitude during the last glacial maximum. Paleoceanography 19:PA4009. doi:10.1029/2004PA001020

An S-I, Ye Z, Hsieh WW (2006) Changes in the leading ENSO modes associated with the late 1970s climate shift: role of surface zonal current. Geophys Res Lett 33:L14609. doi:10.1029/2006GL026604

An S-I, Ham Y-G, Kug J-S, Timmermann A, Choi J, Kang I-S (2010) The inverse effect of annual-mean state and annual-cycle changes on ENSO. J Clim 23:1095–1110

Battisti DS (1988) The dynamics and thermodynamics of a warming event in a coupled tropical atmosphere/ocean model. J Atmos Sci 45:2889–2919

Bejarano L (2006) Coexistence of leading equatorial coupled modes for ENSO. Ph.D. Dissertation, Florida State University

Bjerkness J (1966) A possible response of the atmospheric Hadley circulation to equatorial anomalies of ocean temperature. Tellus 18:820–829

Bjerkness J (1969) Atmospheric teleconnections from the equatorial Pacific. Mon Weather Rev 97:163–172

Blanke B, Neelin JD, Gutzler D (1997) Estimating the effect of stochastic wind stress forcing on ENSO irregularity. J Clim 10:1473–1486

Burgers G, Jin F–F, van Oldenborgh GJ (2005) The simplest ENSO recharge oscillator. Geophys Res Lett 32:L13706. doi:10.1029/2005GL022951

Carton JA, Giese BS (2008) A reanalysis of ocean climate using simple ocean data assimilation (SODA). Mon Weather Rev 136:2999–3017

Carton JA, Giese BS, Grodsky SA (2005) Sea level rise and the warming of the oceans in the simple ocean data assimilation (SODA) ocean reanalysis. J Geophys Res 110:C09006. doi:10.1029/2004JC002817

Chang P, Wang B, Li T, Ji L (1994) Interactions between the seasonal cycle and the Southern Oscillation: frequency entrainment and chaos in an intermediate coupled ocean-atmosphere model. Geophys Res Lett 21:2817–2820

Chang P, Ji L, Li H, Flugel M (1996) Chaotic dynamics versus stochastic processes in El Niño Southern Oscillation in coupled ocean-atmosphere models. Phys D 98:301–320

Choi J, An S-I, Dewitte B, Hsieh W–W (2009) Interactive feedback between the tropical Pacific decadal oscillation and ENSO in a coupled general circulation model. J Clim 22:6597–6611

Choi J, An S-I, Kug J-S, Yeh S-W (2011) The role of mean state on changes in El Niño's flavor. Clim Dyn 37:1205–1215

Delworth TL et al (2006) GFDL's CM2 global coupled climate models. Part I: formulation and simulation characteristics. J Clim 19:643–674

Dewitte B (2000) Sensitivity of an intermediate coupled ocean-atmosphere model of the tropical Pacific to its oceanic vertical structure. J Clim 13:2363–2388

Eckert C, Latif M (1997) Predictability of a stochastically forced hybrid coupled model of El Niño. J Clim 10:1488–1504

Fedorov AV, Philander SGH (2000) Is El Niño changing? Science 288:1997–2002

Fedorov AV, Philander SGH (2001) A stability analysis of tropical ocean-atmosphere interactions: bridging measurements and theory for El Niño. J Clim 14:3086–3101

Galanti E, Tziperman E (2000) ENSO's phase locking to the seasonal cycle in the fast-SST, fast-wave, and mixed-mode regimes. J Atmos Sci 57:2936–2950

Galanti E, Tziperman E, Harrison M, Rosati A, Giering R, Sirkes Z (2002) The equatorial thermocline outcropping-A seasonal control on the tropical Pacific ocean-atmosphere instability strength. J Clim 15:2721–2739

Gu D, Philander SGH (1995) Secular changes of annual and interannual variability in the tropics during the past century. J Clim 8:864–876

Guilyardi E (2006) El Niño-mean state-seasonal cycle interactions in a multi-model ensemble. Clim Dyn 26:329–348

Jin F–F (1996) Tropical ocean-atmosphere interaction, the Pacific cold tongue, and the El Niño-Southern Oscillation. Science 274:76–78

Jin F–F, An S-I (1999) Thermocline and zonal advection feedbacks within the equatorial ocean recharge oscillator model for ENSO. Geophys Res Lett 26:2989–2992

Jin F–F, Neelin DJ, Ghil M (1994) El Niño on the devil's staircase: annual subharmonic steps to chaos. Science 264:70–72

Jin F–F, An S-I, Timmermann A, Zhao J (2003) Strong El Niño events and nonlinear dynamical heating. Geophys Res Lett 30:1120

Jin F–F, Kim ST, Bejarano L (2006) A coupled-stability index of ENSO. Geophys Res Lett 33:L23708. doi:10.1029/2006GL027221

Kim K-Y, Chung C (2001) On the evolution of the annual cycle in the tropical Pacific. J Clim 14:991–994

Kim ST, Jin F–F (2011) An ENSO stability analysis. Part II: results from the twentieth and twenty-first century simulations of the CMIP3 models. Clim Dyn 36:1609–1627

Li T, Hogan TF (1999) The role of the annual-mean climate on seasonal and interannual variability of the tropical Pacific in a coupled GCM. J Clim 12:780–792

Li T, Philander SGH (1996) On the annual cycle of the eastern equatorial Pacific. J Clim 9:2986–2998

Lindzen RS, Nigam S (1987) On the role of sea surface temperature gradients in forcing low-level winds and convergence in the tropics. J Atmos Sci 44:2418–2436

Monterey GI, Levitus S (1997) Seasonal variability of mixed layer depth for the world ocean. NOAA Atlas NESDIS 14, U.S. Gov. Printing Office, 5 p

Moore AM, Kleeman R (1999) Stochastic forcing of ENSO by the intraseasonal oscillation. J Clim 12:1199–1220

Moorthi S, Suarez MJ (1992) Relaxed Arakawa-Schubert: a parameterization of moist convection for general circulation models. Mon Weather Rev 120:978–1002

Rasmusson EM, Carpenter TH (1982) Variations in tropical sea surface temperature and surface wind fields associated with the Southern Oscillation/El Niño. Mon Weather Rev 110:354–384

Stein K, Timmermann A, Schneider N (2011) Phase synchronization of the El Niño-Southern Oscillation with the annual cycle. Phys Rev Lett 107:128501

Timmermann A, Jin F–F (2002) A nonlinear mechanism for decadal El Niño amplitude changes. Geophys Res Lett 29:1003. doi: 10.1029/2001GL013369

Timmermann A, Jin F–F, Abshagen J (2003) A nonlinear theory for El Niño bursting. J Atmos Sci 60:152–165

Timmermann A, Jin F–F, Collins M (2004) Intensification of the annual cycle in the tropical Pacific due to greenhouse warming. Geophys Res Lett 31:L12208. doi:10.1029/2004GL019442

Timmermann A, Lorenz SJ, An S-I, Clement A, Xie S-P (2007a) The effect of orbital forcing on the mean climate and variability of the tropical Pacific. J Clim 20:4147–4159

Timmermann A et al (2007b) The influence of a weakening of the Atlantic meridional overturning circulation on ENSO. J Clim 20:4899–4919

Torrence C, Compo GP (1998) A practical guide to wavelet analysis. Bull Am Meteorol Soc 79:61–78

Tziperman E, Stone L, Cane MA, Jarosh H (1994) El Niño chaos: overlapping of resonances between the seasonal cycle and the Pacific ocean-atmosphere oscillator. Science 264:72–74

Tziperman E, Cane MA, Zebiak SE, Xue Y, Blumenthal B (1998) Locking of El Niño's peak time to the end of the calendar year in the delayed oscillator picture of ENSO. J Clim 11:2191–2199

Wang XL (1994) The coupling of the annual cycle and ENSO over the tropical Pacific. J Atmos Sci 51:1115–1136

Wang B, An S-I (2001) Why the properties of El Niño changed during the late 1970s. Geophys Res Lett 14:3709–3712

Wang B, Barcilon A, Fang Z (1999) Stochastic dynamics of ENSO. J Atmos Sci 56:5–20

Wittenberg AT, Rosati A, Lau N-C, Ploshay JJ (2006) GFDL's CM2 global coupled climate models. Part III: tropical Pacific climate and ENSO. J Clim 19:698–722

Xie S-P (1994) On the genesis of the equatorial annual cycle. J Clim 7:2008–2013

Xie S-P (1995) Interaction between the annual and interannual variations in the equatorial Pacific. J Phys Oceanogr 25:1930–1941

Xie S-P (1997) Stability of equatorially symmetric and asymmetric climates under annual solar forcing. Q J R Meteorol Soc 123:1359–1375

Zebiak SE, Cane MA (1987) A model El Niño-Southern Oscillation. Mon Weather Rev 115:2262–2278

Zelle H, Appeldoorn G, Burgers G, van Oldenborgh GJ (2004) The relationship between sea surface temperature and thermocline depth in the tropical eastern Pacific. J Clim 34:643–655